Nano-Micro Letters

e-ISSN 2150-5551
CN 31-2103/TB

ARTICLE

https://doi.org/10.1007/s40820-025-01793-2

Cite as
Nano-Micro Lett.
(2025) 17:284

Received: 10 March 2025
Accepted: 5 May 2025

Mixed-Dimensional Nanowires/Nanosheet Heterojunction of GaSb/Bi_2O_2Se for Self-Powered Near-Infrared Photodetection and Photocommunication

Guangcan Wang[1], Zixu Sa[1], Zeqi Zang[1], Pengsheng Li[1], Mingxu Wang[1], Bowen Yang[1], Xiaoyue Wang[1], Yanxue Yin[1], Zai-xing Yang[1] ✉

HIGHLIGHTS

- The mixed-dimensional type II heterojunction of GaSb nanowires (NWs) and Bi_2O_2Se nanosheets (NSs) with a built-in electric field of ~ 140 meV is successfully constructed.
- As-fabricated NW/NS and NW array/NS mixed-dimensional heterojunction photodetectors exhibit as-expected high-performance self-powered photodetection behaviors, including ultralow I_{dark} (0.07 and 0.08 pA), superior I_{light}/I_{dark} ratios (82 and 182) and ultrafast photoresponse (< 2/2 and 6/4 ms).
- As-fabricated NW array/NS mixed-dimensional heterojunction self-powered photodetector promises the future imaging and photocommunication.

ABSTRACT With high surface-to-volume ratio, the abundant surface states and high carrier concentration are challenging the near-infrared photodetection behaviors of narrow band gap semiconductors nanowires. In this study, the narrow band gap semiconductor of Bi_2O_2Se nanosheets (NSs) is adopted to construct mixed-dimensional heterojunctions with GaSb nanowires (NWs) for demonstrating the impressive self-powered NIR photodetection. Benefiting from the built-in electric field of ~ 140 meV, the as-constructed NW/NS mixed-dimensional heterojunction self-powered photodetector shows the low dark current of 0.07 pA, high I_{light}/I_{dark} ratio of 82 and fast response times of < 2/2 ms at room temperature. The self-powered photodetector performance can be further enhanced by fabricating the NW array/NS mixed-dimensional heterojunction by using a contact printing technique. The excellent photodetection performance promises the as-constructed NW/NS mixed-dimensional heterojunction self-powered photodetector in imaging and photocommunication.

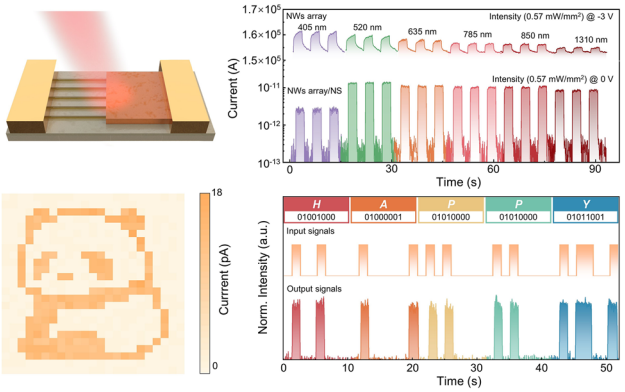

KEYWORDS Near-infrared photodetection; Self-powered photodetection; Mixed-dimensional heterojunction; GaSb nanowire; Bi_2O_2Se nanosheet

✉ Zai-xing Yang, zaixyang@sdu.edu.cn
[1] School of Physics, State Key Laboratory of Crystal Materials, Shandong University, Jinan 250100, People's Republic of China

Published online: 03 June 2025

1 Introduction

Near-infrared (NIR) photodetector has attracted much more attention in remote sensing, medical imaging and environmental monitoring, due to its ability to penetrate biological tissues and the atmosphere [1–12]. With the moderate narrow band gap of 0.72 eV, the highest hole mobility of 850 $cm^2 V^{-1} s^{-1}$ among III–V semiconductors and the broad spectral absorption ability, GaSb nanowires (NWs) have been utilized for near-infrared photodetection in the past decade, which is in forms of photoconductor, field-effect phototransistor and Schottky photodiode [13–17]. With high surface-to-volume ratio, the abundant surface states and high carrier concentration are challenging the NIR photodetection behaviors of GaSb NWs [17–19]. First of all, the surface state will act as the carrier traps, resulting in the bias stress instability of GaSb NW NIR photodetectors [15]. Furthermore, the surface state will cause the famous Fermi level pinning, resulting in the inability to modulate the dark current (I_{dark}) of the NIR photodetector through the metal/semiconductor contact barrier [13, 20]. At the same time, the high carrier concentration will cause the NIR photodetector to suffer from a large I_{dark}, resulting in a low I_{light}/I_{dark} [21].

To date, the surface passivation, van der Waals integration and construction of heterojunction have been developed to optimize the NIR photodetection behaviors of low-dimensional semiconductors [13, 20, 22–24]. Among them, the construction of heterojunction is a popular and meaningful approach, because the built-in electric field and depletion region would be introduced at the semiconductor–semiconductor heterointerfaces by designing reasonably the energy band engineering, benefiting to the quick separation and collection of photogenerated electron–hole pairs, which facilitates the faster photoresponse speed [25–31]. Furthermore, the built-in electric field and depletion region benefit to the success construction of self-powered photodetector, which operates effectively without an external energy source, hold great potential applications in Internet of Things and low power dissipation. At the same time, the I_{dark} will be significantly suppressed and photosensitivity is effectively enhanced due to the barrier at the interfaces and the absence of an external bias, benefiting to the smart photodetection of NIR light [32].

It is worth pointing out that the type II semiconductor heterostructure promotes the separation of photogenerated carriers by directing electrons and holes across the interface in opposite directions [33–35]. This property makes the type II heterojunctions ideal candidates for ultrasensitive and self-powered photodetectors [36–41]. With narrow band gap of 0.8 eV, Bi_2O_2Se nanosheets (NSs) are adopted to construct mixed-dimensional type II heterojunctions with GaSb NWs for demonstrating the impressive self-powered NIR photodetection, optical imaging and photocommunication in this work [42, 43]. Benefiting from the built-in electric field, the as-fabricated NW/NS heterojunction photodetector exhibits excellent self-powered photodetection performance, that is, the I_{dark} is as low as 0.07 pA, the I_{light}/I_{dark} ratio is as high as 82, and the response times are as fast as < 2/2 ms, which significantly outperform the NW and NS photodetectors. Furthermore, the self-powered photodetection performance is further improved by constructing NW array/NS heterojunction photodetector. The fabricated NW array/NS heterojunction self-powered photodetector exhibits low I_{dark} of 0.08 pA, high I_{light}/I_{dark} ratio of 182 and fast optical response times of 6/4 ms. In the end, the fabricated NW array/NS heterojunction also enables self-powered imaging and photocommunication capabilities. These results demonstrate that the construction of GaSb NW/Bi_2O_2Se NS mixed-dimensional heterostructures promises the next-generation high-performance self-powered NIR photodetection.

2 Experimental Section

2.1 Growth of GaSb NWs and Bi_2O_2Se NSs

GaSb NWs are prepared by using a surfactant-assisted CVD method in a dual-zone horizontal tube furnace [44]. High-purity GaSb powder (99.999%) is placed in the upstream zone, a Si/SiO_2 growth substrate coated with a 1-nm Pd catalyst is positioned in the downstream zone, and sulfur powder (99.99%) is placed between the two zones. The precursor vapor from the upstream zone is carried to the downstream zone by using hydrogen gas (99.999% purity). The CVD system is evacuated to 6×10^{-3} Torr and purged with 200 sccm of H_2 for 30 min prior to heating. Upon reaching the designated time, the source and substrate heaters are turned off simultaneously, allowing the system to cool to room temperature under a hydrogen flow.

https://doi.org/10.1007/s40820-025-01793-2

The Bi_2O_2Se NSs are prepared on the mica by CVD method in a dual-zone horizontal tube furnace [45]. Source powder of Bi_2O_3 (0.1 g, 99.99%) is placed in the heating center of the first zone, and Bi_2Se_3 powder (0.01 g, 99.99%) is placed 6 cm upstream. The freshly cleaved mica is placed 6 cm upstream of the heating center in the second zone. Argon (200 sccm, 99.999%) with a tube pressure maintained at 60 Torr is employed as the carrier gas to transport the precursors onto a mica surface for the growth of Bi_2O_2Se NSs. The temperatures in the two zones are set as 690 and 560 °C for 40 min to obtain the Bi_2O_2Se NSs. After the growth process, the system is subsequently cooled to room temperature while maintaining a flow of argon gas.

2.2 Fabrication of GaSb/Bi_2O_2Se Mixed-Dimensional Heterojunctions Photodetectors

First, for a single GaSb NW photodetector, the as-prepared NWs are suspended in an ethanol solution using ultrasonication and subsequently transferred onto Si substrates with a 50-nm SiO_2 layer via drop casting. For NW array photodetectors, the ordered GaSb NWs are transferred onto Si substrates with a 50-nm SiO_2 layer using a contact printing technique. Subsequently, the prepared Bi_2O_2Se NS is transferred from mica onto a SiO_2/Si substrate with GaSb NW or NW array using a wet transfer method, supported by polymethyl methacrylate (PMMA) in a 1% dilute HF solution and finally cleaned with acetone. Finally, the contact electrodes are patterned using standard electron beam lithography, followed by the deposition of 50-nm Ni metal electrodes through a thermal evaporation system.

2.3 Characterization of GaSb/Bi_2O_2Se Mixed-Dimensional Heterojunctions and Photodetectors

The morphology of the as-prepared GaSb NWs and Bi_2O_2Se NSs is characterized using a microscope (Olympus microscope BX53 M) and scanning electron microscopy (SEM, KYKY-EM6900). A scanning probe microscope (Horiba Bruker Multimode 8) equipped with atomic force microscopy (AFM) and Kelvin probe force microscopy (KPFM) modules is used to study the material thickness and surface potential. The photodetection performance of the as-prepared photodetectors is measured using an Agilent B1500A semiconductor analyzer connected to a probe station at room temperature. Diode lasers are used as light sources for photodetection measurements.

3 Results and Discussion

3.1 Design and Construction of Mixed-dimensional NW/NS Heterojunctions

GaSb NWs and Bi_2O_2Se NSs are prepared by chemical vapor deposition (CVD) method in a dual-zone tube furnace. The detailed experimental procedures are described in "Methods" section. SEM image in Fig. 1a shows that the as-prepared GaSb NWs have uniform diameter and smooth surface. Optical microscopy (OM) image reveals that the as-prepared Bi_2O_2Se NSs exhibit regular square morphology with size up to approximately 20 μm. X-ray diffraction (XRD) patterns (Fig. 1b) confirm that the GaSb NWs have a pure zinc-blende crystal structure (JCPDS card No. 07–0215), while Bi_2O_2Se NSs exhibit tetragonal crystal phase (JCPDS card No. 25–1463). The as-prepared GaSb NWs and Bi_2O_2Se NSs are then adopted to construct mixed-dimensional heterojunctions by PMMA-assisted wet transfer method, as reported in the literature [42]. Figure 1c displays the OM and SME images of as-constructed GaSb/Bi_2O_2Se NW/NS and NW array/NS mixed-dimensional heterojunctions, demonstrating the high-quality contact between NWs and NSs. AFM is then employed to measure the diameter of GaSb NW and the thickness of Bi_2O_2Se NS in the as-constructed GaSb/Bi_2O_2Se NW/NS mixed-dimensional heterojunction, as shown in Fig. 1d, e. As a result, the diameter is 25 nm and the thickness is 30 nm. Furthermore, the Kelvin probe force microscopy (KPFM) is adopted to measure the surface potentials of GaSb NW and Bi_2O_2Se NS, demonstrating the Fermi level difference. The measured area is as same as the AFM image in the inset of Fig. 1d. In this case, the potential curve is obtained from the cross of NW and NS, as depicted by the white line in the inset of Fig. 1f. As shown in Fig. 1f, Bi_2O_2Se NS exhibits a higher surface potential than GaSb NW, with a Fermi level difference of approximately 140 meV. The schematic of energy band alignment is then shown in Fig. 1g-i, benefiting to the explanation of photogenerated carrier transfer behavior at the heterostructure interface. As reported in the studies, the band gaps of GaSb NW and Bi_2O_2Se NS are approximately 0.72 and

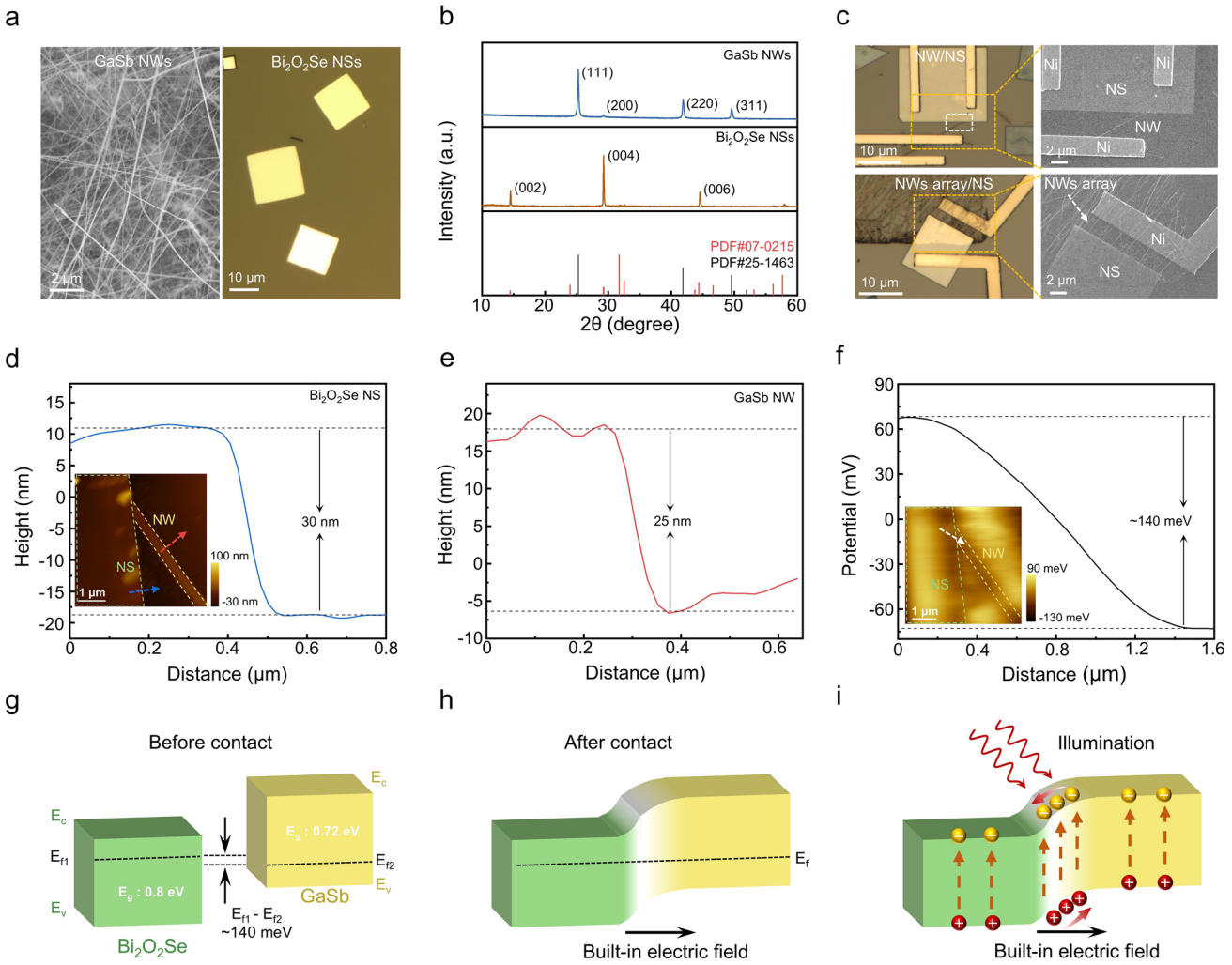

Fig. 1 Construction of GaSb/Bi_2O_2Se mixed-dimensional NW/NS heterojunctions for self-powered photodetection. **a, b** SEM, OM images and XRD patterns of GaSb NWs and Bi_2O_2Se NSs, respectively. **c** OM and SEM images of NW/NS and NW array/NS heterojunction, respectively. **d, e** Height profiles of Bi_2O_2Se NS and GaSb NW. Inset is the AFM image of GaSb/Bi_2O_2Se NW/NS heterojunction. **f** Surface potential difference profile of GaSb/Bi_2O_2Se NW/NS heterojunction. **g–i** Schematic of the self-powered GaSb/Bi_2O_2Se NW/NS heterojunction photodetector (the E_c, E_v and E_f are the conduction band minimum, valance band maximum and Fermi level, respectively)

0.8 eV, respectively [14, 20]. When GaSb and Bi_2O_2Se come into contact, the higher Fermi level of Bi_2O_2Se facilitates the transfer of electrons into GaSb, leading to the thermal equilibrium and unified Fermi level. At the same time, the band will bend at the interface, forming a useful type II heterojunction. It is worth pointing out that the built-in electric field and depletion region form at the interface, which directs from Bi_2O_2Se NS to GaSb NW. In this case, under the illumination with wavelength shorter than 1310 nm, the photogenerated electron–hole pairs will be separated and collected quickly without an external energy source, which facilitates the self-powered photodetection behaviors with faster photoresponse speed and reduced I_{dark}. In summary, the as-constructed GaSb/Bi_2O_2Se mixed-dimensional heterojunctions promise the next-generation self-powered high-performance NIR photodetection.

3.2 Photodetection Behaviors of Mixed-dimensional NW/NS Heterojunction

After the success in constructing NW/NS heterojunction, the corresponding photodetection behaviors are then studied in Fig. 2. Figure 2a presents the I–V curves of NW,

https://doi.org/10.1007/s40820-025-01793-2

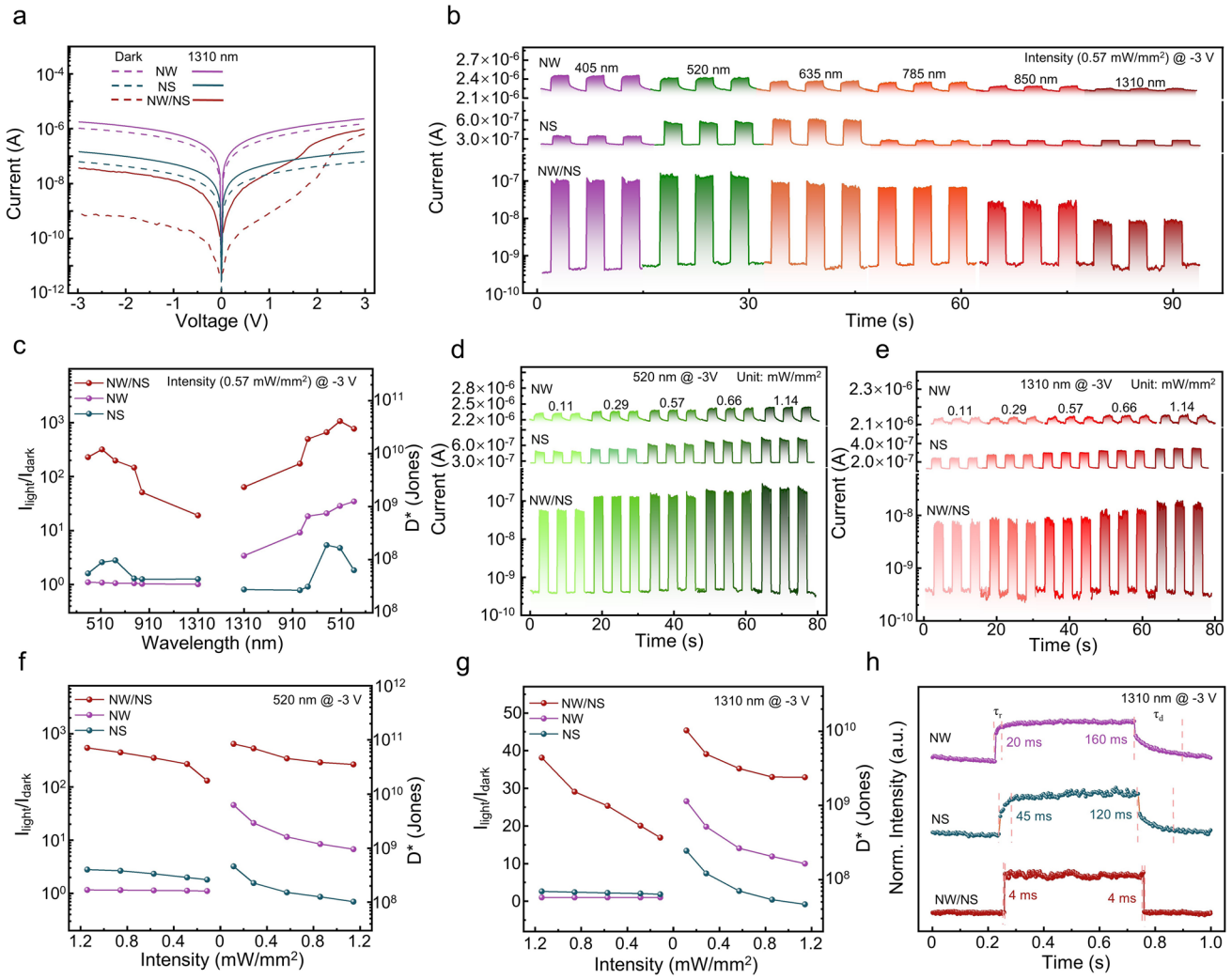

Fig. 2 Photodetection behaviors of GaSb NW, Bi_2O_2Se NS and GaSb/Bi_2O_2Se mixed-dimensional NW/NS heterojunction. **a** I–V characteristics of the NW, NS and NW/NS mixed-dimensional heterojunction photodetectors in dark and under the illumination of 1310-nm laser with power intensity of 0.57 mW mm^{-2}. **b** Wavelength-dependent temporal photoresponse of the NW, NS and NW/NS heterojunction photodetectors. **c** I_{light}/I_{dark} ratio, D* and response time of the NW, NS and NW/NS heterojunction photodetectors under the illuminations of 405–1310-nm laser with power intensity of 0.57 mW mm^{-2}. **d, e** I–t curves of the NW, NS and NW/NS heterojunction photodetectors under the illumination of 520- and 1310-nm lasers, respectively. **f, g** I_{light}/I_{dark} ratio and D* of the NW, NS and NW/NS heterojunction photodetectors under the illumination of 405- and 1310-nm laser, respectively. **h** Response times of the NW, NS and NW/NS heterojunction photodetectors

NS and NW/NS heterojunction photodetectors in dark and under the illumination of 1310-nm laser with an intensity of 0.57 mW mm^{-2}. It is worth pointing out that both of the as-fabricated GaSb NW and Bi_2O_2Se NS photodetectors exhibit Ohmic contacts, which rules out the influence of the Schottky barrier for the heterostructure, as depicted in Fig. S1. Under −3 V bias, the NW/NS heterojunction photodetector shows the lowest I_{dark} of 0.5 nA and the highest I_{light}/I_{dark} ratio of 20. Figure 2b shows the wavelength-dependent photoresponse of the three photodetectors under −3 V bias. Benefiting from the narrow band gaps of GaSb and Bi_2O_2Se, the as-fabricated NW, NS and NW/NS heterojunction photodetectors all exhibit broadband photodetection capability. Notably, the I_{dark} is significantly suppressed after constructing NW/NS heterojunction. As shown in Fig. 2c, as expected, due to the suppressed I_{dark}, the I_{light}/I_{dark} ratio of the heterojunction photodetector is improved across the wavelength range of 405–1310 nm. The I_{light}/I_{dark} ratio of NW/NS heterojunction photodetector is substantially enhanced by factors of 294 and 122 compared to NW and

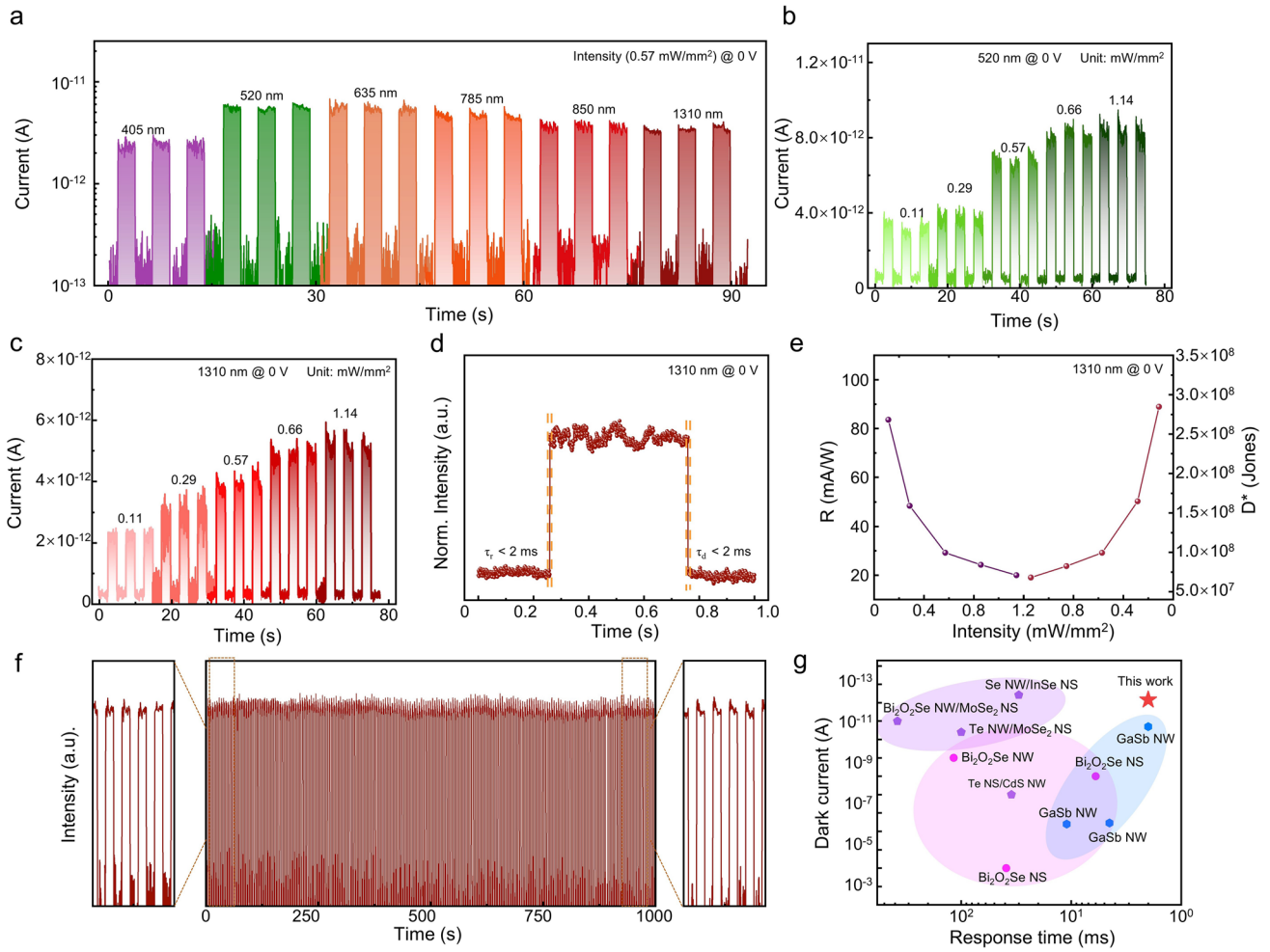

Fig. 3 Self-powered NIR photodetection behaviors of GaSb/Bi_2O_2Se mixed-dimensional NW/NS heterojunction. **a** Wavelength-dependent photoresponse of the NW/NS heterojunction self-powered photodetector. **b, c** Intensity-dependent photoresponse under the illuminations of 520- and 1310-nm lasers. **d-f** Response time, R, D* and long-term stability of NW/NS heterojunction self-powered NIR photodetector. **g** I_{dark} and response time comparison between this work and other photodetectors previously reported in the studies, including GaSb NW, Bi_2O_2Se NS, mixed-dimensional heterojunctions. References to the selected work can be found in Table S1

NS photodetectors. Two critical parameters of responsivity (R) and detectivity (D*) are also optimized in Figs. S2 and 2c. *R* can be defined as I_{ph}/(PA), and *D** can be defined as $RA^{1/2}/(2eI_{dark})^{1/2}$, in which *P* is the incident power density, *A* is the effective irradiated area, e is the electronic charge, and I_{ph} is defined as $I_{light}-I_{dark}$ [46]. In this case, the values of *R* and *D** are 2.3×10^3, 3.2, 9.7×10^2 A W^{-1} and 1.0×10^9, 1.7×10^8, 4.1×10^{10} Jones for NW, NS and NW/NS heterojunction photodetectors, respectively.

The intensity-dependent photoresponse of the three photodetectors under the illuminations of 520- and 1310-nm lasers is shown in Figs. 2d, e and S3. The I_{light} of all three devices increases linearly with the increase in the incident light intensity. Among them, the I_{light} of NW/NS heterojunction photodetector increases from 59.7 and 7.7 nA to 247.7 and 17.3 nA under the illuminations of 520- and 1310-nm lasers with the intensity increases from 0.11 to 1.14 mW mm^{-2}. Figure 2f, g shows the intensity-dependent I_{light}/I_{dark} ratio and D* of the three photodetectors. The I_{light}/I_{dark} ratio increases with the increase in the laser intensity, while the D* decreases as the laser intensity increases. Notably, the NW/NS heterojunction photodetector achieves a maximum I_{light}/I_{dark} ratio of 545 and 38, and a *D** of 8.4×10^{10} and 1.0×10^{10} Jones, respectively, under the illuminations of 520 and 1310 nm, further demonstrating the decreased I_{dark} and excellent photosensitivity. The response time, including

https://doi.org/10.1007/s40820-025-01793-2

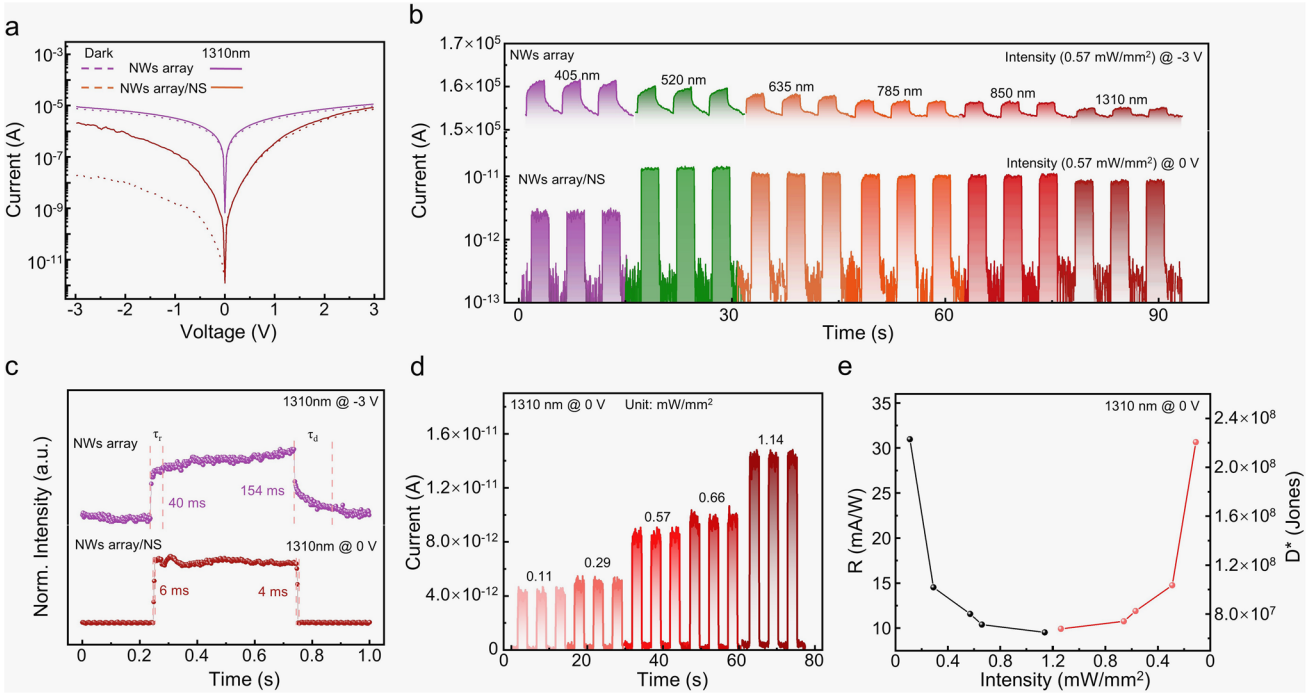

Fig. 4 Photodetection behaviors of GaSb array and GaSb/Bi_2O_2Se mixed-dimensional NW array/NS heterojunction. **a** I–V characteristic curves of the NW array and NW array/NS heterojunction photodetectors in dark and under the illumination of 1310-nm laser (0.57 mW mm^{-2}). **b** Wavelength-dependent temporal photoresponse of the NW array and NW array/NS heterojunction photodetector. **c** Response time of the NW array and NW array/NS heterojunction photodetectors under the illumination of 1310-nm laser. **d** Self-powered photodetection behaviors of NW array/NS mixed-dimensional heterojunction photodetector under the illumination of 1310-nm laser. **e** *R* and *D** of the self-powered NW array/NS heterojunction photodetector versus the incident light (1310-nm) intensity

the rise time (τ_r) and the decay time (τ_d), is another critical parameter of photodetectors. It refers to the time required for photocurrent to rise from 10 to 90% or fall from 90 to 10% [47]. As shown in Fig. 2h, the NW/NS heterojunction photodetector achieves τ_r/τ_d values of 4/4 ms, much shorter than the 20/160 and 45/120 ms of NW and NS photodetectors, respectively. In short, the as-constructed NW/NS mixed-dimensional heterojunction promises the next-generation high-performance photodetectors.

The built-in electric field facilitates the self-powered NIR photodetection behaviors of NW/NS heterojunction photodetector, which are detailedly studied in Fig. 3. As shown in Fig. 3a, NW/NS heterojunction photodetector exhibits as-expected broadband photodetection capability under no external bias voltage, along with extremely low I_{dark} of 0.07 pA. The dark current fluctuation is caused by the resolution limitation of semiconductor analyzer. The self-powered photodetection behaviors of the NW/NS heterojunction photodetector are further studied under the illumination of 520- and 1310-nm lasers, as shown in Fig. 3b, c. The I_{light} increases from 3.8 and 2.5 to 9.5 and 5.9 pA under the illuminations of 520- and 1310-nm lasers with the intensity increases from 0.11 to 1.14 mW mm^{-2}, while the I_{dark} is maintained at a level of 0.07 pA. The I_{light}/I_{dark} ratio increases with the increase in the laser intensity, referring the superior photosensitivity of the NW/NS heterojunction. In self-powered mode, the photodetector exhibits τ_r and τ_d of <2 ms each, as illustrated in Fig. 3d. The NIR photodetection performance of the NW/NS heterojunction photodetector is further evaluated by *R* and *D**, as shown in Fig. 3e. Under the illumination of 1310 nm with power intensity of 0.11 mW mm^{-2}, the *R* and *D** reach 84 mA W^{-1} and 2.85×10^8 Jones, respectively. Operation stability is a critical metric of photodetectors. Figure 3f exhibits the photoresponse of the NW/NS heterojunction self-powered photodetector over an operation time of 1000 s. No significant I_{light} attenuation demonstrates the excellent operational stability. The as-fabricated NW/NS heterojunction photodetector is compared with other photodetectors with similar material systems or configurations in Fig. 3g. Clearly, the as-fabricated NW/NS heterojunction

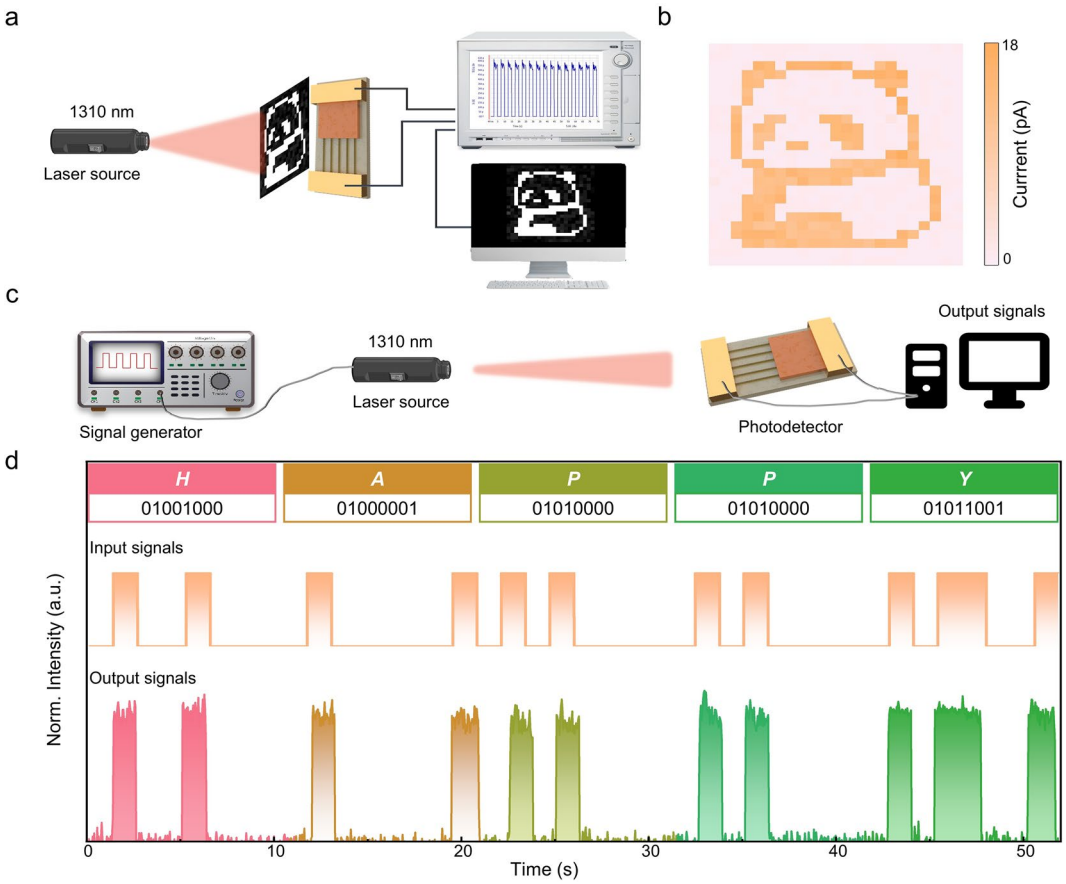

Fig. 5 Imaging and optical communication functions of GaSb/Bi_2O_2Se mixed-dimensional NW array/NS heterojunction self-powered NIR photodetector. **a** Schematic illustration of the NW array/NS heterojunction photodetector for imaging. **b** Photodetection imaging demonstration of a panda. **c** Schematic diagram of ASCII code signal transportation system. **d** Photocommunication demonstration of ASCII codes of "HAPPY"

photodetector outperforms most counterparts in terms of fast response speed and exceptionally low I_{dark}. In summary, the NW/NS mixed-dimensional heterojunction photodetector exhibits outstanding self-powered NIR photodetection performance.

3.3 Photodetection Behaviors of Mixed-dimensional NW Array/NS Heterojunction

Ordered NW array has been considered promising candidates for the large-scale integration of optoelectronic devices [57, 58]. The ordered NW array is obtained by the reported contact printing technology [59, 60]. Then, the photodetection behaviors of NW array and the NW array/NS mixed-dimensional heterojunction photodetectors are studied in Fig. 4. Figure 4a exhibits the I–V curves of NW array and NW array/NS mixed-dimensional heterojunction photodetectors in dark and under the illumination of 1310-nm laser with an intensity of 0.57 mW mm^{-2}. Under −3 V bias, the NW/NS heterojunction photodetector shows the lowest I_{dark} of 32 nA and the highest I_{light}/I_{dark} ratio of 60. The I_{dark} of the NW array/NS heterojunction photodetector is significantly reduced, approximately 600 times lower than that of the NW array photodetector. The wavelength-dependent photoresponse of the NW array and NW array/NS heterojunction photodetectors is shown in Figs. 4b and S4a, further demonstrating the improved I_{light}/I_{dark} ratio and decreased I_{dark} (0.08 pA). More importantly, the increased contact area between GaSb NWs and Bi_2O_2Se NS results in a larger photocurrent, which is twice as large as that of the NW/NS photodetector. The τ_r and τ_d of the NW array/NS heterojunction self-powered photodetector are 6 and 4 ms, significantly lower than the τ_r/τ_d

 https://doi.org/10.1007/s40820-025-01793-2

of 30/20 ms under −3 V bias and τ_r/τ_d of 40/154 ms for the NW array photodetector (Figs. 4c and S4b). Under the illumination of 1310-nm laser, the self-powered NIR photodetection behavior of the NW array/NS heterojunction photodetector is further investigated in Figs. 4d and S4c. With increasing incident light intensity from 0.11 to 1.14 mW mm^{-2}, the I_{light} rises proportionally from 4.7 to 14 pA, leading to a maximum I_{light}/I_{dark} ratio of 182. The NIR photodetection performance of the as-fabricated self-powered NW array/NS heterojunction photodetector is evaluated by calculating the R and D^*, as shown in Fig. 4e. With the 1310-nm light of 0.11 mW mm^{-2}, the R is up to 31 mA W^{-1}, while D^* is up to 2.21×10^8 Jones. In a word, the splendid photodetection performance confirms the effective strategy of constructing the NW array/NS mixed-dimensional heterojunction for the self-powered NIR photodetection.

3.4 Imaging and Photocommunication of Mixed-dimensional NW Array/NS Heterojunction

The ultrafast photoresponse and superior photosensitivity of as-constructed NW array/NS mixed-dimensional heterojunction self-powered photodetector hold great promise in imaging and photocommunication. Figure 5a provides a conceptual diagram illustrating the imaging principle of the NW array/NS heterojunction photodetector. Figure 5b displays the single-pixel imaging result, showing a clear "panda" image and highlighting the NW array/NS heterojunction photodetector's significant potential for self-powered imaging. Figure 5c depicts a schematic diagram of the NW array/NS mixed-dimensional heterojunction self-powered photodetector integrated into a NIR photocommunication system. A signal generator encodes the ASCII message "HAPPY" into a voltage signal, which is then used to control laser emission. Upon receiving the optical signal, the NW array/NS mixed-dimensional heterojunction self-powered photodetector produces a photocurrent signal corresponding to the ASCII message "HAPPY" as illustrated in Fig. 5d. This photocurrent signal is decoded into the message "HAPPY" effectively demonstrating the feasibility of NIR photocommunication.

4 Conclusion

In conclusion, the high-performance self-powered NIR photodetectors are achieved by constructing the mixed-dimensional heterojunction of GaSb NWs and Bi_2O_2Se NS, promising the photodetection imaging and photocommunication. Due to the formation of a ~ 140 mV Fermi level difference, the as-fabricated NW/NS and NW array/NS mixed-dimensional heterojunction photodetectors exhibit ultralow I_{dark} (0.07 and 0.08 pA) and ultrafast photoresponse (< 2/2 and 6/4 ms). Furthermore, the as-fabricated NW array/NS mixed-dimensional heterojunction self-powered photodetector successfully demonstrated its potential for applications in imaging and photocommunication. Overall, this study promises the as-constructed mixed-dimensional GaSb/Bi_2O_2Se NW/NS heterojunction, a novel platform for next-generation high-performance self-powered NIR photodetection, imaging and photocommunication.

Acknowledgements We acknowledge the Natural Science Foundation of Shandong Province (Nos. ZR2022JQ05 and ZR2024MF010).

Author's Contribution ZY conceived the project. ZY and GW designed the experiments and wrote the manuscript. GW, ZS and ZZ contributed to the photodetection measurement. PL contributed to the growth of GaSb NWs and Bi_2O_2Se NSs. MW contributed to the XRD measurement. BY contributed to the SEM measurement. XW contributed to the AFM measurement. YY contributed to the KPFM measurement. All authors have discussed the results and commented on the manuscript.

Declarations

Conflict of interest The authors declare no interest conflict. They have no known competing financial interests or personal relationships that could have appeared to influence the work reported in this paper.

Supplementary Information The online version contains supplementary material available at https://doi.org/10.1007/s40820-025-01793-2.

References

1. J. Chen, L. Li, P. Gong, H. Zhang, S. Yin et al., A submicrosecond-response ultraviolet-visible-near-infrared broadband photodetector based on 2D tellurosilicate $InSiTe_3$. ACS Nano **16**(5), 7745–7754 (2022). https://doi.org/10.1021/acsnano.1c11628
2. L. Zeng, D. Wu, J. Jie, X. Ren, X. Hu et al., Van der waals epitaxial growth of mosaic-like 2D platinum ditelluride layers for room-temperature mid-infrared photodetection up to 10.6 μm. Adv. Mater. **32**(52), 2004412 (2020). https://doi.org/10.1002/adma.202004412
3. J. Li, Z. Wang, Y. Wen, J. Chu, L. Yin et al., High-performance near-infrared photodetector based on ultrathin Bi_2O_2Se nanosheets. Adv. Funct. Mater. **28**(10), 1706437 (2018). https://doi.org/10.1002/adfm.201706437
4. D. Wu, Z. Mo, X. Li, X. Ren, Z. Shi et al., Integrated mid-infrared sensing and ultrashort lasers based on wafer-level Td-WTe_2 Weyl semimetal. Appl. Phys. Rev. **11**(4), 041401 (2024). https://doi.org/10.1063/5.0204248
5. W. Pan, M. Tan, Y. He, H. Wei, B. Yang, Organic amine-bridged quasi-2D perovskite/PbS colloidal quantum dots composites for high-gain near-infrared photodetectors. Nano Lett. **22**(6), 2277–2284 (2022). https://doi.org/10.1021/acs.nanolett.1c04569
6. F. Wang, F. Hu, M. Dai, S. Zhu, F. Sun et al., A two-dimensional mid-infrared optoelectronic retina enabling simultaneous perception and encoding. Nat. Commun. **14**(1), 1938 (2023). https://doi.org/10.1038/s41467-023-37623-5
7. Y. Wang, L. Peng, J. Schreier, Y. Bi, A. Black et al., Silver telluride colloidal quantum dot infrared photodetectors and image sensors. Nat. Photonics **18**(3), 236–242 (2024). https://doi.org/10.1038/s41566-023-01345-3
8. D. Wu, C. Guo, L. Zeng, X. Ren, Z. Shi et al., Phase-controlled van der Waals growth of wafer-scale 2D $MoTe_2$ layers for integrated high-sensitivity broadband infrared photodetection. Light Sci. Appl. **12**(1), 5 (2023). https://doi.org/10.1038/s41377-022-01047-5
9. J. Qiao, F. Feng, S. Song, T. Wang, M. Shen et al., Perovskite quantum dot-Ta_2NiSe_5 mixed-dimensional van der waals heterostructures for high-performance near-infrared photodetection. Adv. Funct. Mater. **32**(13), 2110706 (2022). https://doi.org/10.1002/adfm.202110706
10. J. Zha, M. Luo, M. Ye, T. Ahmed, X. Yu et al., Infrared photodetectors based on 2D materials and nanophotonics. Adv. Funct. Mater. **32**(15), 2111970 (2022). https://doi.org/10.1002/adfm.202111970
11. Q. Wang, Y. Wen, K. Cai, R. Cheng, L. Yin et al., Nonvolatile infrared memory in MoS_2/PbS van der waals heterostructures. Sci. Adv. **4**(4), eaap7916 (2018). https://doi.org/10.1126/sciadv.aap7916
12. L. Zeng, W. Han, X. Ren, X. Li, D. Wu et al., Uncooled mid-infrared sensing enabled by chip-integrated low-temperature-grown 2D $PdTe_2$ Dirac semimetal. Nano Lett. **23**(17), 8241–8248 (2023). https://doi.org/10.1021/acs.nanolett.3c02396
13. D. Liu, F. Liu, Y. Liu, Z. Pang, X. Zhuang et al., Schottky-contacted high-performance GaSb nanowires photodetectors enabled by lead-free all-inorganic perovskites decoration. Small **18**(16), 2200415 (2022). https://doi.org/10.1002/smll.202200415
14. F. Liu, X. Zhuang, M. Wang, D. Qi, S. Dong et al., Lattice-mismatch-free construction of III-V/chalcogenide core-shell heterostructure nanowires. Nat. Commun. **14**(1), 7480 (2023). https://doi.org/10.1038/s41467-023-43323-x
15. Z. Sa, F. Liu, X. Zhuang, Y. Yin, Z. Lv et al., Toward high bias-stress stability P-type GaSb nanowire field-effect-transistor for gate-controlled near-infrared photodetection and photocommunication. Adv. Funct. Mater. **33**(38), 2304064 (2023). https://doi.org/10.1002/adfm.202304064
16. J. Sun, M. Peng, Y. Zhang, L. Zhang, R. Peng et al., Ultrahigh hole mobility of Sn-catalyzed GaSb nanowires for high speed infrared photodetectors. Nano Lett. **19**(9), 5920–5929 (2019). https://doi.org/10.1021/acs.nanolett.9b01503
17. Z.-X. Yang, N. Han, M. Fang, H. Lin, H.-Y. Cheung et al., Surfactant-assisted chemical vapour deposition of high-performance small-diameter GaSb nanowires. Nat. Commun. **5**, 5249 (2014). https://doi.org/10.1038/ncomms6249
18. Z. Ren, P. Wang, K. Zhang, W. Ran, J. Yang et al., Short-wave near-infrared polarization sensitive photodetector based on GaSb nanowire. IEEE Electron Device Lett. **42**(4), 549–552 (2021). https://doi.org/10.1109/LED.2021.3061705
19. J. Sun, M. Han, Y. Gu, Z.-X. Yang, H. Zeng, Recent advances in group III–V nanowire infrared detectors. Adv. Opt. Mater. **6**(18), 1800256 (2018). https://doi.org/10.1002/adom.201800256
20. G. Wang, F. Liu, R. Chen, M. Wang, Y. Yin et al., Tunable contacts of Bi_2O_2Se nanosheets MSM photodetectors by metal-assisted transfer approach for self-powered near-infrared photodetection. Small **20**(8), 2306363 (2024). https://doi.org/10.1002/smll.202306363
21. X. Zhang, R. Li, Y. Yu, F. Dai, R. Jiang et al., Dark Current mechanisms and suppression strategies for infrared photodetectors based on two-dimensional materials. Laser Photonics Rev. **18**(5), 2300936 (2024). https://doi.org/10.1002/lpor.202300936
22. H. Wang, Z. Li, D. Li, P. Chen, L. Pi et al., Van der waals integration based on two-dimensional materials for high-performance infrared photodetectors. Adv. Funct. Mater. **31**(30), 2103106 (2021). https://doi.org/10.1002/adfm.202103106
23. K. Zhang, Z. Ren, H. Cao, L. Li, Y. Wang et al., Near-infrared polarimetric image sensors based on ordered sulfur-passivation GaSb nanowire arrays. ACS Nano **16**(5), 8128–8140 (2022). https://doi.org/10.1021/acsnano.2c01455
24. J. Li, C. Duan, Q. Zhang, C. Chen, Q. Wen et al., Self-generated buried submicrocavities for high-performance

near-infrared perovskite light-emitting diode. Nano Micro Lett. **15**(1), 125 (2023). https://doi.org/10.1007/s40820-023-01097-3

25. Y. Han, S. Jiao, X. Zhang, P. Rong, Y. Zhao et al., Bipolar modulation in a self-powered ultra-wide photodetector based on Bi_2Se_3/AlInAsSb heterojunction for wavelength-sensitive imaging and encrypted optical communication. Adv. Mater. **37**(7), 2416935 (2025). https://doi.org/10.1002/adma.202416935
26. C. Li, Z. Wu, C. Zhang, S. Peng, J. Han et al., Self-powered photodetector with high performance based on all-2D $NbSe_2$/$MoSe_2$ van der waals heterostructure. Adv. Opt. Mater. **11**(22), 2300905 (2023). https://doi.org/10.1002/adom.202300905
27. M. Liu, J. Wei, L. Qi, J. An, X. Liu et al., Photogating-assisted tunneling boosts the responsivity and speed of heterogeneous WSe_2/Ta_2NiSe_5 photodetectors. Nat. Commun. **15**(1), 141 (2024). https://doi.org/10.1038/s41467-023-44482-7
28. S. Yang, P. Luo, F. Wang, T. Liu, Y. Zhao et al., Van der waals epitaxy of Bi_2Te_2Se/Bi_2O_2Se vertical heterojunction for high performance photodetector. Small **18**(6), 2105211 (2022). https://doi.org/10.1002/smll.202105211
29. G. Rao, X. Wang, Y. Wang, P. Wangyang, C. Yan et al., Two-dimensional heterostructure promoted infrared photodetection devices. InfoMat **1**(3), 272–288 (2019). https://doi.org/10.1002/inf2.12018
30. R. Cheng, F. Wang, L. Yin, Z. Wang, Y. Wen et al., High-performance, multifunctional devices based on asymmetric van der Waals heterostructures. Nat. Electron. **1**(6), 356–361 (2018). https://doi.org/10.1038/s41928-018-0086-0
31. P. Lei, J. Wang, Y. Gao, C. Hu, S. Zhang et al., An electrochromic nickel phosphate film for large-area smart window with ultra-large optical modulation. Nano-Micro Lett. **15**(1), 34 (2023). https://doi.org/10.1007/s40820-022-01002-4
32. L. Han, M. Yang, P. Wen, W. Gao, N. Huo et al., A high performance self-powered photodetector based on a 1D Te–2D WS_2 mixed-dimensional heterostructure. Nanoscale Adv. **3**(9), 2657–2665 (2021). https://doi.org/10.1039/D1NA00073J
33. J. Ahn, K. Ko, J.H. Kyhm, H.S. Ra, H. Bae et al., Near-infrared self-powered linearly polarized photodetection and digital incoherent holography using WSe_2/$ReSe_2$ van der waals heterostructure. ACS Nano **15**(11), 17917–17925 (2021). https://doi.org/10.1021/acsnano.1c06234
34. J. Kistner-Morris, A. Shi, E. Liu, T. Arp, F. Farahmand et al., Electric-field tunable Type-I to Type-II band alignment transition in $MoSe_2$/WS_2 heterobilayers. Nat. Commun. **15**(1), 4075 (2024). https://doi.org/10.1038/s41467-024-48321-1
35. F. Wang, Z. Wang, K. Xu, F. Wang, Q. Wang et al., Tunable GaTe-MoS_2 van der waals p-n junctions with novel optoelectronic performance. Nano Lett. **15**(11), 7558–7566 (2015). https://doi.org/10.1021/acs.nanolett.5b03291
36. J. Chen, Z. Zhang, Y. Ma, J. Feng, X. Xie et al., High-performance self-powered ultraviolet to near-infrared photodetector based on WS_2/InSe van der Waals heterostructure. Nano Res. **16**(5), 7851–7857 (2023). https://doi.org/10.1007/s12274-022-5323-1
37. F. Wang, T. Zhang, R. Xie, A. Liu, F. Dai et al., Next-generation photodetectors beyond van der waals junctions. Adv. Mater. **36**(3), e2301197 (2024). https://doi.org/10.1002/adma.202301197
38. Y. Mao, T. Deng, Y. Li, F. He, The GeSe/SnSe heterojunction photodetector with self-powered characteristics and high infrared response performance. Appl. Phys. Lett. **124**(18), 181106 (2024). https://doi.org/10.1063/5.0188990
39. P. Luo, F. Zhuge, F. Wang, L. Lian, K. Liu et al., PbSe quantum dots sensitized high-mobility Bi_2O_2Se nanosheets for high-performance and broadband photodetection beyond 2 μm. ACS Nano **13**(8), 9028–9037 (2019). https://doi.org/10.1021/acsnano.9b03124
40. H. Ma, H. Fang, X. Xie, Y. Liu, H. Tian et al., Optoelectronic synapses based on MXene/violet phosphorus van der waals heterojunctions for visual-olfactory crossmodal perception. Nano-Micro Lett. **16**(1), 104 (2024). https://doi.org/10.1007/s40820-024-01330-7
41. X. Tang, H. Jiang, Z. Lin, X. Wang, W. Wang et al., Wafer-scale vertical 1D GaN nanorods/2D MoS_2/PEDOT: PSS for piezophototronic effect-enhanced self-powered flexible photodetectors. Nano-Micro Lett. **17**(1), 56 (2024). https://doi.org/10.1007/s40820-024-01553-8
42. Q. Fu, C. Zhu, X. Zhao, X. Wang, A. Chaturvedi et al., Ultrasensitive 2D Bi_2O_2Se phototransistors on silicon substrates. Adv. Mater. **31**(1), e1804945 (2019). https://doi.org/10.1002/adma.201804945
43. L. Sun, Y. Xu, T. Yin, R. Wan, Y. Ma et al., Van der Waals heterostructure of Bi_2O_2Se/$MoTe_2$ for high-performance multifunctional devices. Nano Energy **119**, 109047 (2024). https://doi.org/10.1016/j.nanoen.2023.109047
44. X. Zhuang, Z. Sa, J. Zhang, M. Wang, M. Xu et al., An amorphous native oxide shell for high bias-stress stability nanowire synaptic transistor. Adv. Sci. **10**(31), 2302516 (2023). https://doi.org/10.1002/advs.202302516
45. W. Wang, Y. Zhang, W. Wang, M. Luo, Y. Meng et al., Orientation-engineered 2D electronics on van der waals dielectrics. Matter **7**(6), 2236–2249 (2024). https://doi.org/10.1016/j.matt.2024.04.013
46. W. Cheng, S. Wu, J. Lu, G. Li, S. Li et al., Self-powered wide-narrow bandgap-laminated perovskite photodetector with bipolar photoresponse for secure optical communication. Adv. Mater. **36**(5), 2307534 (2024). https://doi.org/10.1002/adma.202307534
47. B. Zhang, Z. Ao, X. Lan, J. Zhong, F. Zhang et al., Self-rolled-up WSe_2 one-dimensional/two-dimensional homojunctions: enabling high-performance self-powered polarization-sensitive photodetectors. Nano Lett. **24**(25), 7716–7723 (2024). https://doi.org/10.1021/acs.nanolett.4c01745
48. Y. Yin, Y. Guo, D. Liu, C. Miao, F. Liu et al., Substrate-free chemical vapor deposition of large-scale III–V nanowires for high-performance transistors and broad-spectrum photodetectors. Adv. Opt. Mater. **10**(6), 2102291 (2022). https://doi.org/10.1002/adom.202102291
49. Z. Sa, F. Liu, D. Liu, M. Wang, J. Zhang et al., Ag-catalyzed GaSb nanowires for flexible near-infrared photodetectors. J.

Semicond. **43**(11), 112302 (2022). https://doi.org/10.1088/1674-4926/43/11/112302

50. U. Khan, Y. Luo, L. Tang, C. Teng, J. Liu et al., Controlled vapor–solid deposition of millimeter-size single crystal 2D Bi_2O_2Se for high-performance phototransistors. Adv. Funct. Mater. **29**(14), 1807979 (2019). https://doi.org/10.1002/adfm.201807979
51. U. Khan, L. Tang, B. Ding, Y. Luo, S. Feng et al., Catalyst-free growth of atomically thin Bi_2O_2Se nanoribbons for high-performance electronics and optoelectronics. Adv. Funct. Mater. **31**(31), 2101170 (2021). https://doi.org/10.1002/adfm.202101170
52. J. Han, C. Fang, M. Yu, J. Cao, K. Huang, A high-performance Schottky photodiode with asymmetric metal contacts constructed on 2D Bi_2O_2Se. Adv. Electron. Mater. **8**(7), 2100987 (2022). https://doi.org/10.1002/aelm.202100987
53. Z. Chen, J. Huang, M. Yang, X. Liu, Z. Zheng et al., Bi_2O_2Se nanowire/$MoSe_2$ mixed-dimensional polarization-sensitive photodiode with a nanoscale ultrafast-response channel. ACS Appl. Mater. Interfaces **15**(25), 30504–30516 (2023). https://doi.org/10.1021/acsami.3c05283
54. S. Liu, L. Zhang, X. Wang, High-performance 1D CdS/2D Te heterojunction photodetector. J. Phys. Conf. Ser. **2809**(1), 012034 (2024). https://doi.org/10.1088/1742-6596/2809/1/012034
55. H. Shang, H. Chen, M. Dai, Y. Hu, F. Gao et al., A mixed-dimensional 1D Se-2D InSe van der Waals heterojunction for high responsivity self-powered photodetectors. Nanoscale Horiz. **5**(3), 564–572 (2020). https://doi.org/10.1039/c9nh00705a
56. J. You, Z. Jin, Y. Li, T. Kang, K. Zhang et al., Epitaxial growth of 1D Te/2D $MoSe_2$ mixed-dimensional heterostructures for high-efficient self-powered photodetector. Adv. Funct. Mater. **34**(10), 2311134 (2024). https://doi.org/10.1002/adfm.202311134
57. C. Jia, Z. Lin, Y. Huang, X. Duan, Nanowire electronics: from nanoscale to macroscale. Chem. Rev. **119**(15), 9074–9135 (2019). https://doi.org/10.1021/acs.chemrev.9b00164
58. J.-L. Wang, M. Hassan, J.-W. Liu, S.-H. Yu, Nanowire assemblies for flexible electronic devices: recent advances and perspectives. Adv. Mater. **30**(48), 1803430 (2018). https://doi.org/10.1002/adma.201803430
59. Z. Fan, J.C. Ho, Z.A. Jacobson, R. Yerushalmi, R.L. Alley et al., Wafer-scale assembly of highly ordered semiconductor nanowire arrays by contact printing. Nano Lett. **8**(1), 20–25 (2008). https://doi.org/10.1021/nl071626r
60. Z.X. Yang, L. Liu, S. Yip, D. Li, L. Shen et al., Complementary metal oxide semiconductor-compatible, high-mobility, ⟨111⟩-oriented GaSb nanowires enabled by vapor-solid-solid chemical vapor deposition. ACS Nano **11**(4), 4237–4246 (2017). https://doi.org/10.1021/acsnano.7b01217

 https://doi.org/10.1007/s40820-025-01793-2